Electronic distributions of Al-Mn and Al-Mn-Si alloys

1992 J. Phys.: Condens. Matter 4 1057

(http://iopscience.iop.org/0953-8984/4/4/016)

J. Phys.: Condens. Matter 4 (1992) 1057–1068. Printed in the UK

Electronic distributions of Al–Mn and Al–Mn–Si alloys

Esther Belin†, Joseph Kojnok‡, Anne Sadoc§, Agnès Traverse‖, Mireille Harmelin¶, Claire Berger†† and Jean-Marie Dubois‡‡

† Laboratoire de Chimie Physique (Unité associée au CNRS 176), 11 rue Pierre et Marie Curie, 75231 Paris Cédex, France

‡ Laboratory of Surface and Interface Physics, Eötvos University, 4-6 Muzéum krt. H-1088 Budapest, Hungary

§ Laboratoire d'Utilisation du Rayonnement Electromagnetique, Bâtiment 209D, Université Paris-Sud, 91405 Orsay Cédex, France

‖ Centre de Spectrométrie Nucléaire et de Spectrométrie de Masse, Bâtiment 108, 91405 Orsay Cédex, France

¶ Centre d'Etudes de Chimie Métallurgique (CNRS), 15 rue Georges Urbain, 94407 Vitry Cédex, France

†† Laboratoire d'Etudes des Propiétés Electroniques des Solides (CNRS), BP166X, 38042 Grenoble Cédex, France

‡‡ Laboratoire de Sciences et Génie des Matériaux Métalliques (Unité associée au CNRS 159), Parc de Saurupt, 54042 Nancy Cédex, France

Received 29 July 1991, in final form 24 September 1991

Abstract. Electronic distributions of various symmetries have been investigated for both valence and conduction bands in a series of Al–Mn and Al–Mn–Si alloys of different structural states (amorphous, quasi-crystalline or crystalline) and Mn concentrations ranging from 14 to 22 at.%. Experiments have been carried out by means of soft-x-ray emission and photoabsorption spectroscopies. This allowed us to provide a complete description of the valence band states and to confirm the progressive opening of a small gap in the Al–sp DOS at the Fermi level with increasing Mn concentration in the alloys. At a given Mn concentration the gap is wider for the quasi-crystalline phase than for its crystalline counterpart.

1. Introduction

Besides the increase in research on the atomic structure of the so-called quasi-crystals, much interest has also arisen in their electronic properties both theoretically (see, e.g., Marcus 1986, Smith and Ashcroft 1987, Fujiwara 1989, 1990, Matsuda *et al* 1990, Fujiwara and Yokokawa 1991) and experimentally (see, e.g., Bruwiller *et al* 1987, Ederer *et al* 1988, Traverse *et al* 1988, Macko *et al* 1989, Wagner *et al* 1989, Gozlan *et al* 1990, Berger *et al* 1991). To understand these properties, knowledge of the electronic structure and therefore the distributions of the valence and conduction band states may be helpful.

In a previous paper (Belin and Traverse 1991), we showed that Al 3p electronic distributions of the valence band in $Al_{100-x}Mn_x$ alloys are somewhat different according to their structural states: crystalline, amorphous or quasi-crystalline. Special attention was paid to the occupied density-of-states (DOS) distributions at the Fermi level E_F. We pointed out that

Table 1. Structural state, preparation technique and studied SXS spectra for various Al–Mn and Al–Mn–Si alloys: RS, rapid solidification; RS*, rapid solidification + annealing; S, sputtering after rapid solidification; IBMM, ion beam mixing of multilayers.

Alloy	Structural state	Preparation technique	Al $L_{2,3}$	Mn Lα	Al K	Mn K
Al	c		×		×	
Mn	c			×		×
$Al_{73}Mn_{21}Si_6$	c	RS*	×	×		×
	i	RS	×	×		×
$Al_{86}Mn_{14}$	c	RS, IBMM	×	×	×	×
	i	RS, IBMM	×	×	×	×
	a	RS, IBMM	×	×	×	×
$Al_{85}Mn_{15}$	a	S		×	×	×
$Al_{83}Mn_{17}$	a	S	×	×		
$Al_{81}Mn_{19}$	a	RS, IBMM	×	×		
$Al_{80}Mn_{20}$	d	RS	×	×	×	×
$Al_{79}Mn_{21}$	a	IBMM	×	×		
$Al_{78}Mn_{22}$	d	RS	×	×		
Al_2O_3	c		×		×	

(i) for a given Mn content, the DOS at E_F decreases from the crystal to the quasi-crystal and

(ii) with increasing Mn content in the alloy, whatever the structural state may be, there is a continuous evolution from a metallic-like behaviour to a less metallic-like behaviour as revealed by the progressive opening of a small gap at the Fermi level.

These observations are consistent with results deduced from resistivity measurements (see references in the work of Belin and Traverse (1991)). These first results provided the incentive for continuing the experiments in order to describe as completely as possible the DOS of these materials and, in particular, states with different symmetries in the valence band together with those of the conduction band.

The aim of this paper is to report an experimental analysis of Al 3s and Mn 3d occupied and also Al p and Mn p empty states distributions for the same Al–Mn and Al–Mn–Si alloys as studied previously. Both soft-x-ray emission spectroscopy (SXES) and soft-x-ray photoabsorption spectroscopy (SXAS) experiments were carried out; in fact, such measurements allow us to investigate separately either full (SXES) or empty (SXAS) electronic distributions of a selected angular momentum around each kind of atom in the solid. Note that the information obtained here concerns the bulk material.

In the following, we describe briefly in section 2 the experimental procedures and give in section 3 the results. In section 4 the data are discussed comparatively for the quasi-crystalline phases and the related crystalline phases and also in connection with the Al 3p distributions. A picture of the total valence band is thus deduced.

2. Experimental procedure

Various Al–Mn and Al–Mn–Si single-phase alloys have been investigated: crystalline (c), quasi-crystalline (i or d for the icosahedral and decagonal structures, respectively) or amorphous (a). Table 1 indicates their composition, structural state, preparation

mode and the spectra which have been studied. The structural states of all the samples were very carefully controlled by techniques such as transmission electron microscopy, x-ray or neutron diffraction, and extended x-ray absorption fine structure (see references in Shechtman *et al* (1984), Dubois *et al* (1986), Harmelin (1988), Traverse *et al* (1988) and Berger *et al* (1991)). Thin films as well as solid targets were used for both SXES and SXAS experiments.

The Al 3s and Mn 3d–4s distributions were obtained through analysis of the Al $L_{2,3}$ (valence band → Al $2p_{3/2}$ level) and Mn Lα (valence band → Mn $2p_{3/2}$ level) emission spectra, and the Al p and Mn p empty-state distributions through analysis of the Al K (Al 1s → conduction band) and Mn K (Mn 1s → conduction band) photoabsorption spectra. Several spectrometers were necessary to obtain the different spectra.

For the emission experiments, water-cooled samples were the target of the x-ray tube; they were irradiated by either incoming electrons (Al) or photons (Mn). To obtain the Al $L_{2,3}$ emission spectra, we used a Johan-type vacuum spectrometer (equipped with a grating of 600 lines mm^{-1} with a radius of curvature of 2 m), whose energy resolution in the experimental range is about 0.3 eV. The Mn Lα spectra were obtained with a spectrometer equipped with a KAP crystal with a radius of curvature of 0.5 m; the experimental resolution is also about 0.3 eV. In both cases the spectrometers were provided with electronic detectors of entrance slits placed on the focalization cylinders of the grating or crystal; successive scans along the Rowland cylinder were necessary to achieve convenient accuracy.

The photoabsorption experiments were carried out with either a Johan-type vacuum spectrometer equipped with a W anode or the synchrotron radiation facilities at Laboratoire d'Utilisation du Rayonnement Electromagnétique. For the Al K photoabsorption we used a spectrometer with a SiO_2 $10\bar{1}0$ plate with a radius of 0.5 m, the experimental energy resolution of which is about 0.2 eV in the analysed range and also an ACO storage ring with a two-crystal quartz monochromator, the experimental energy resolution of which was about 0.5 eV. The Mn K photoabsorption was obtained with a DCI storage ring using a Si(331) channel-cut monochromator and a slit of 1 mm so that the experimental resolution is about 0.55 eV.

Binding energy measurements of Al and Mn $2p_{3/2}$ core levels were also performed in an x-ray photoemission spectrograph (XPS technique) with an accuracy of ±0.1 eV for Al and ±0.2 eV for Mn.

3. Results

The experimental electronic distributions of the different samples can be compared because the SXS curves are adjusted on the same energy scale, namely the binding energy scale. The Fermi level E_F, taken as the origin, is located on the x-ray transition energy scale within ±0.2 eV owing to the measurement of the binding energies of the inner levels involved in the x-ray transitions which we analyse. No shift in the Fermi level was observed in the alloys with respect to the pure metals within ±0.2 eV.

The emission curves, corresponding to the Al 3s and Mn 3d occupied DOS, are normalized at the same height between the maximum intensity value and the bottom of the curves where the variation in the intensity is negligible. The Al K photoabsorption curves, corresponding to the Al p empty DOS, are normalized between the bottom before the edge, where the variation in the intensity is negligible, and the intensity at 4 eV from E_F; indeed up to $E_F - 4$ eV no oxide contribution may be involved in the spectra. The

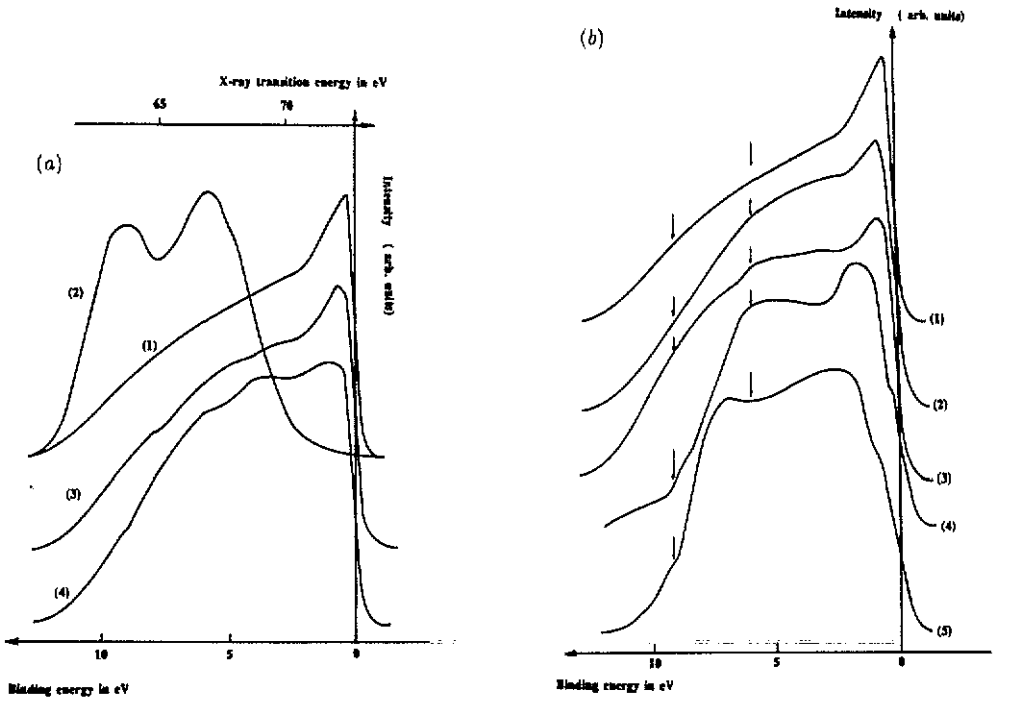

Figure 1. (*a*) Al 3s distribution states curves in pure Al (curve 1), Al_2O_3 (curve 2) and in crystalline (curve 3) and quasi-crystalline (curve 4) $Al_{73}Mn_{21}Si_6$. The curve corresponding to Al_2O_3 is given on the x-ray transition energy scale. The curves (except curve 2) are arbitrarily shifted along the intensity axis. (*b*) Al 3s distribution states curves in pure Al (curve 1), and in c-$Al_{86}Mn_{14}$ (curve 2), i-$Al_{86}Mn_{14}$ (curve 3), d-$Al_{80}Mn_{20}$ (curve 4) and d-$Al_{78}Mn_{22}$ (curve 5) alloys. The curves are arbitrarily shifted along the intensity axis.

Mn K photoabsorption curves, which correspond to empty DOS of p character, are normalized between the bottom of the curves just before the jump and about 15 eV from E_F.

We show the Al 3s distributions for pure Al (curve 1), c-$Al_{73}Mn_{21}Si_6$ (curve 3) and i-$Al_{73}Mn_{21}Si_6$ alloys (curve 4) in figure 1(*a*), and for pure Al (curve 1), c-$Al_{86}Mn_{14}$ (curve 2), i-$Al_{86}Mn_{14}$ (curve 3), d-$Al_{80}Mn_{20}$ (curve 4) and d-$Al_{78}Mn_{22}$ (curve 5) phases in figure 1(*b*). The Al 3s distribution curve for Al_2O_3 consists of two wide peaks; it is also presented in figure 1(*a*), on the x-ray transition energy scale, and the maxima are indicated by vertical arrows in figure 1(*b*). This makes it possible to ascertain where Al 3s distributions curves might be affected by oxidation. The shape of all the curves up to $E_F + 4$ eV is only due to Al; beyond this energy range, the various curves may contain an oxide contribution which we cannot account for. The oxide contribution is not dominant in the spectra; it is 6–10% depending on the sample.

The c-$Al_{73}Mn_{21}Si_6$ emission band edge is very abrupt; as for pure Al, a prominent peak is observed near E_F but it is less marked. The same is true for c-$Al_{86}Mn_{14}$ (figure 1(*b*)). This peak is still present in the quasi-crystalline alloys but it is less sharp; it progressively tends to vanish with increasing Mn concentration in the alloys. The slopes of the edges of all the Al–Mn–Si and Al–Mn alloys are rather abrupt; thus, the intensities at E_F, which are indicated in table 2, are measured within ±2%. It should be noted that

Table 2. Intensity at E_F from occupied Al 3s distribution curves for various Al–Mn and Al–Mn–Si alloys.

Alloy	Intensity at E_F (%) ± 2
c-$Al_{73}Mn_{21}Si_6$	45
i-$Al_{73}Mn_{21}Si_6$	36
c-$Al_{86}Mn_{14}$	48
i-$Al_{86}Mn_{14}$	40
d-$Al_{80}Mn_{20}$	33
d-$Al_{78}Mn_{22}$	29

for the decagonal phases, the edges have two steps; a change in slope occurs at 0.4 eV for d-$Al_{80}Mn_{20}$ and at 1.0 eV for d-$Al_{78}Mn_{22}$.

Our data for the Al 3s distributions in the Al–Mn and Al–Mn–Si alloys are nearly consistent with previous results from Bruwiller *et al* (1987) and Ederer *et al* (1988).

Figure 2, curves 1, 2, 3, 4 and 5, are the K photoabsorption curves for pure Al, c-$Al_{86}Mn_{14}$, i-$Al_{86}Mn_{14}$, d-$Al_{80}Mn_{20}$ and a-$Al_{86}Mn_{14}$, respectively. The curve corresponding to Al_2O_3 is also presented. The wide peak situated at about $E_F - 6$ eV for pure Al is hardly noticeable for c-$Al_{86}Mn_{14}$; it is not seen in the quasi-crystalline and amorphous phases. For i-$Al_{86}Mn_{14}$ and d-$Al_{80}Mn_{20}$, a broad peak is observed at about $E_F - 9.5$ eV; the difference between the intensities of these structures for the icosahedral and decagonal alloys is not significant, since in this energy range oxide may contribute to the curves. In any case, the curve for the amorphous phase which shows a different fine structure may be affected by oxide contribution beyond $E_F - 6$ eV. More significant is the fact that the intensity at E_F decreases when going from crystalline to icosahedral, decagonal and amorphous alloys as the edges of the corresponding Al p empty bands are progressively repelled from E_F. The values given in table 3 are measured within ±2%.

The Mn Lα bands of Mn, c-$Al_{73}Mn_{21}Si_6$, i-$Al_{86}Mn_{14}$, d-$Al_{80}Mn_{20}$ and a-$Al_{83}Mn_{17}$ are shown in figure 3, curves 1, 2, 3, 4 and 5, respectively. These bands display the same shape for pure Mn and for the alloys whatever the structural state may be. Table 4 gives the full width at half-maximum (FWHM), the distance δ of the maximum with respect to the Fermi level and the intensity h at E_F according to the atomic structure and the concentration of Mn in the sample. A narrowing of the FWHM of the Lα band with respect to that of the pure metal is observed in the alloys. The FWHM decreases as the Mn concentration increases in the alloy and as one goes from crystalline to icosahedral, or from decagonal to amorphous phases. At the same time, the maximum of the Lα distribution tends to be closer to E_F and the DOS at E_F tends to increase.

Figure 4, curves 1, 2, 3, 4, 5, 6 and 7, are the K photoabsorption curves for Mn, c-$Al_{86}Mn_{14}$, i-$Al_{86}Mn_{14}$, d-$Al_{80}Mn_{20}$, a-$Al_{85}Mn_{15}$, c-$Al_{73}Mn_{21}Si_6$ and i-$Al_{73}Mn_{21}Si_6$ alloys, respectively. Curve 1 shows an arctan-like jump followed by a flat plateau until 5 eV from E_F and a monotonic increase in intensity. The edges of the curves corresponding to the alloys exhibit roughly the same shape but are slightly steeper than for the metal; there is no plateau, the intensity increases monotonically except in icosahedral and decagonal alloys where, at about 5–6 eV from E_F, there is an enhancement of intensity.

It should be noted that no differences due to the different techniques used for the preparation of the studied samples arise in the results.

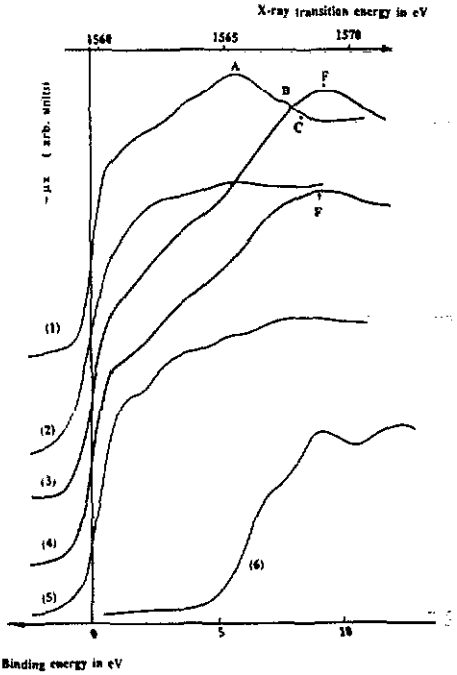

Figure 2. Al p empty distribution curves in pure Al (curve 1), Al_2O_3 (curve 6) and in c-$Al_{86}Mn_{14}$ (curve 2), i-$Al_{86}Mn_{14}$ (curve 3), d-$Al_{80}Mn_{20}$ (curve 4) and a-$Al_{86}Mn_{14}$ (curve 5) alloys. The curve corresponding to Al_2O_3 is given on the x-ray transition energy scale. The curves are arbitrarily shifted along the μx axis.

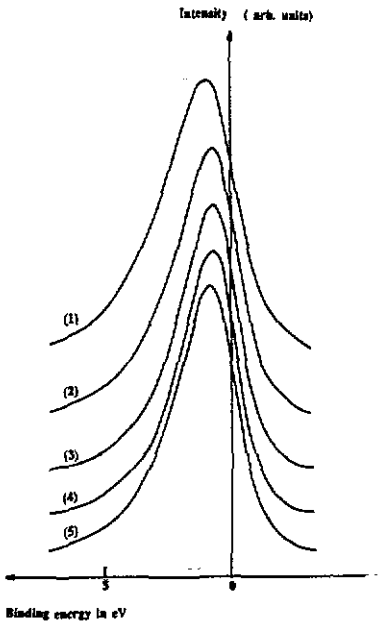

Figure 3. Mn 3d–4s state distribution curves in pure Mn (curve 1), and in c-$Al_{73}Mn_{21}Si_6$ (curve 2), i-$Al_{86}Mn_{14}$ (curve 3), d-$Al_{80}Mn_{20}$ (curve 4) and a-$Al_{83}Mn_{17}$ (curve 5) alloys. The curves are arbitrarily shifted along the intensity axis.

Table 3. intensity at E_F from empty Al p distribution curves for various Al–Mn alloys.

Alloy	Intensity at E_F (%) ± 2
c-$Al_{86}Mn_{14}$	46
i-$Al_{86}Mn_{14}$	38
a-$Al_{86}Mn_{14}$	22
d-$Al_{80}Mn_{20}$	33

4. Discussion

4.1. Valence band distributions

We have already pointed out that our experiments give the variation in Al 3s and Mn 3d–4s DOS of the valence band. For Mn, because of transition probabilities, the Lα curve reflects mainly the 3d states distribution.

Since we have achieved different curves on the same energy scale, it is possible to adjust the Mn 3d, Al 3s and Al 3p DOS. These latter were obtained previously for the same alloys (Belin and Traverse 1991). The adjustment is shown in figures 5, 6 and

Table 4. Mn Lα FWHM, distance δ from E_F and intensity h at E_F for several Al–Mn and Al–Mn–Si alloys according to their Mn concentration and structural state.

Alloy	Structural state	FWHM (eV) ± 0.1	δ (eV) ± 0.1	h (%) ± 1
Mn	c	3.4	1.0	70
$Al_{73}Mn_{21}Si_6$	c	3.0	0.7	78
$Al_{73}Mn_{21}Si_6$	i	2.9	0.7	80
$Al_{86}Mn_{14}$	c	3.0	0.8	79
$Al_{86}Mn_{14}$	i	2.8	0.8	75
$Al_{83}Mn_{17}$	a	2.8	0.8	72
$Al_{81}Mn_{19}$	a	2.7	0.6	74
$Al_{77}Mn_{23}$	i	2.9	0.7	86
$Al_{80}Mn_{20}$	d	2.75	0.7	75.5
$Al_{80}Mn_{20}$	a	2.75	0.6	82
$Al_{78}Mn_{22}$	d	2.9	0.7	83

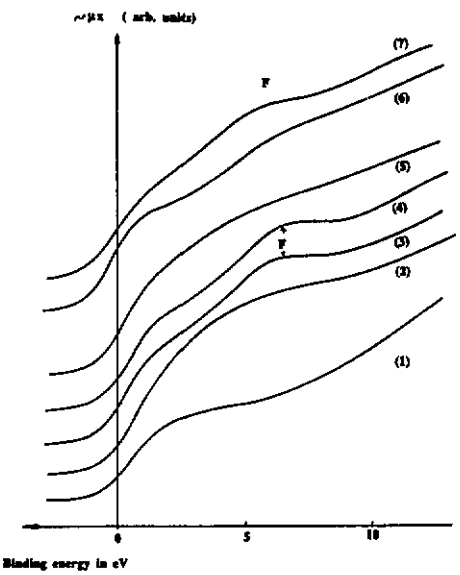

Figure 4. Mn p empty state distribution curves in pure Mn (curve 1) and in c-$Al_{86}Mn_{14}$ (curve 2), i-$Al_{86}Mn_{14}$ (curve 3), d-$Al_{80}Mn_{20}$ (curve 4), a-$Al_{85}Mn_{15}$ (curve 5), c-$Al_{73}Mn_{21}Si_6$ (curve 6) and i-$Al_{73}Mn_{21}Si_6$ (curve 7) alloys. The curves are arbitrarily shifted along the μx axis.

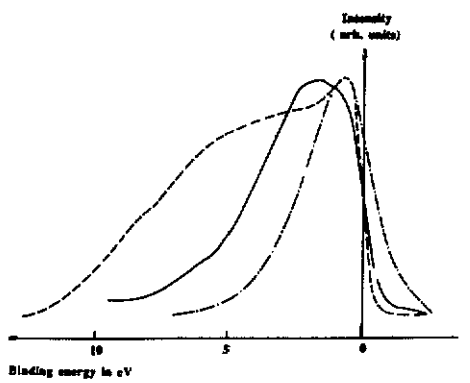

Figure 5. Valence state distribution for c-$Al_{86}Mn_{14}$: — —, Al 3s distributions; ——, Al 3p distributions; —·—, Mn 3d–4s distributions.

7, respectively, for c-$Al_{86}Mn_{14}$, i-$Al_{86}Mn_{14}$ and d-$Al_{80}Mn_{20}$. Similar figures could be obtained from the other samples which we have analysed. The general features are: when the binding energies are increasing from E_F, one finds first Mn 3d states which interact with the Al 3s and Al 3p states; then the states are Al sp hybridized; finally there are almost Al s pure states in the low-lying part of the band.

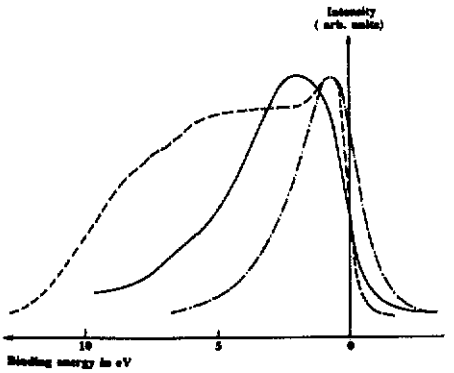

Figure 6. Valence state distribution for i-$Al_{86}Mn_{14}$: — —, Al 3s distributions; ——, Al 3p distributions; —·—, Mn 3d–4s distributions.

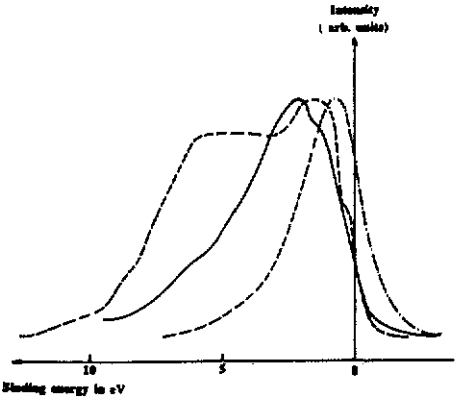

Figure 7. valence state distribution for d-$Al_{80}Mn_{20}$: — —, Al 3s distributions; ——, Al 3p distributions; —·—, Mn 3d–4s distributions.

Let us concentrate on the DOS at E_F. The behaviour of the Al 3s states of the various alloys is similar to that of the Al 3p reported previously (Belin and Traverse 1991); with increasing Mn in the alloy, the intensity at E_F decreases whatever the structural state but, for a given Mn concentration, this intensity is lower when going from crystalline to icosahedral, decagonal and amorphous phases. This indicates that the Al 3s and Al 3p states in Al–Mn or Al–Mn–Si alloys are totally hybridized at E_F. Let us recall that this behaviour of the DOS at E_F was found to be consistent with the fact that the resistivity increases from crystalline to icosahedral and decagonal alloys of the same nominal composition (Belin and Traverse (1991) and references therein). These new experimental results confirm the progressive opening of a small gap in the Al sp DOS at E_F in Al–Mn or Al–Mn–Si alloys as the Mn concentration increases.

For the less Mn concentrated alloys, it is to note that, except at E_F, in the range E_F + 2–2.5 eV, the interaction seems to be stronger between Mn 3d and Al 3s states than between Mn 3d and Al 3p; indeed, the maximum of the Al 3p distributions is then less close to E_F than that of the Al 3s. When the Mn content increases in the alloy, we have already noticed that the Al 3s and Al 3p bands are repelled from E_F whereas the Mn 3d band tends to approach E_F; thus the Al 3s and Mn 3d distribution maxima are no longer superimposed and the interaction between these states is progressively less achieved. This is clearly seen for d-$Al_{80}Mn_{20}$ (figure 7) compared with i-$Al_{86}Mn_{14}$ (figure 6).

Whereas the Al DOS decreases when the Mn content increases in the alloys, the Mn DOS increases and is rather noticeable: this Mn d increase is driven by the Mn concentration, whatever the structure, icosahedral, decagonal or amorphous. However, because our measurements are normalized as explained above, they cannot give absolute values of the DOS. Absolute values have been obtained using specific heat measurements by Berger *et al* (1991) for a-$Al_{85}Mn_{15}$, a-$Al_{83}Mn_{17}$ and i-$Al_{86}Mn_{14}$; it should be noted that a total DOS increase was estimated with a relative order of magnitude similar to that found here for the d-state increase. Our data also show that the Fermi level is not located at the maximum of the Mn 3d distribution; thus there is no experimental evidence for the existence of a virtual bound state in the alloys as was suggested by several workers

(see, e.g., Mayou *et al* 1988). While the present results agree with resistivity measurements which can be understood by the gap opening in the Al s–p DOS at E_F, no information can be deduced from the Mn DOS concerning the magnetism of the Al–Mn or Al–Mn–Si alloys. However, the enhanced magnetic properties with increasing Mn concentration observed by Gozlan *et al* (1991) in the a- and i-AlMn phases, also correspond to the enhanced d DOS measured here. All this outlines the important role played by the Mn d states at E_F, hybridized with Al s and p states.

Furthermore, we have observed that the prominent peak close to E_F progressively tends to vanish when the Mn content increases in the quasi-crystalline alloys. It is known that Al can be described in a free-electron model. The Al $L_{2,3}$ band is parabolic-like; therefore, near E_F, the interaction between the core 1s hole and the conduction electrons is responsible for the large enhancement in intensity and the curve in this region is $(E - E_0)$ α-like with $\alpha = \frac{1}{2}$ (E_0 is the energy at Γ in the first Brillouin zone). We have seen that this prominent peak has a rather strong intensity in crystalline phases for Mn contents of both 14 at.% and 21 at.%. The electronic properties of these alloys are expected to be well described in the free-electron model; in fact, c-$Al_{86}Mn_{14}$ has a resistivity comparable with that of a good metal.

The progressive decrease in the intensity of the many-body feature near E_F in the quasi-crystalline alloys when the Mn content is increased shows that the alloys in this energy range cannot be described within the same electronic model as Al. In this range, Mn d electrons are present which tend to repel the Al 3s–3p towards high binding energies from E_F; thus the valence electrons are progressively less 'Al-like' and acquire an increasingly more localized character. This suggests that the free-electron model is less and less adapted to the description of the Al–Mn quasi-crystalline electronic properties with increasing Mn concentration.

In a calculation of the DOS performed for disordered systems with a great number of neighbours in a Bethe lattice approximation model, Mayou *et al* (1986) found that at E_F the s–p DOS decreases inside the d band owing to the creation of a pseudo-gap at the top of the d band. These workers point out that the local environment does not play the major role in the electronic structure but that the chemical environment introduces strong modifications of the DOS. They also remark that some of the features induced by hybridization effects seem to be quite dependent on the topology of the material. Irrespective of whether the model is used for amorphous or liquid alloys, our results for Al–Mn and Al–Mn–Si alloys concerning the existence of a gap at E_F and fine structure in the Al DOS for the different phases are in agreement with these theoretical predictions.

Using the same structural approximation, Cyrot-Lackmann *et al* (1988) have studied s–d hybridization effects for disordered systems, using a tight-binding model and a random-phase approximation. They analysed the DOS of transition-metal-based amorphous alloys and showed that, when the concentration of the transition metal is increased in a normal metal such as Al, it is possible to create a material which behaves as a semiconductor provided that strong chemical short-range order exists. As an example they predict the formation of a pseudo-gap in $Al_{100-x}Mn_x$ for x about 20%, although for disordered alloys this model agrees with our present and previous (Belin and Traverse 1991) experimental observations. Let us recall that the model above presents essentially chemical aspects, it could be refined by taking structural effects more into account.

More recently a calculation of the valence band state distribution has been performed by Fujiwara (1989, 1990) for crystalline α-$Al_{114}Mn_{24}$ which is considered to be a good approximant of the icosahedral quasi-crystalline Al–Mn phase. The calculated DOS

presents a highly spiky structure. The projected DOS on Mn or Al α sites shows that intense Mn d states lie close to E_F superposed on Mn s states of very low intensity; Al p states of noticeable intensity are found over about 12 eV with the maximum of the distribution located at about $E_F + 2$ eV, while Al s states cover about the same energy extent as the Al p but are weak near E_F and intense beyond $E_F + 2$–3 eV. This calculation predicts that a pseudo-gap is located in the middle of the Mn 3d band and that E_F lies in the middle of the pseudo-gap; it also emphasizes the Al 3s–Mn 4s hybridization responsible for the deep tail in the DOS towards high binding energies. Thus, no virtual bound state arises from this theoretical approach.

At first sight, our experimental results also agree with this picture of the valence band distributions since Mn states are found in the vicinity of E_F, Al 3p in the middle of the band and Al 3s at high binding energies and since a small gap is observed at E_F. However, the agreement is not so good for the Al 3s states distributions; the calculated Al 3s DOS predicts a very weak intensity at E_F and beyond the spiky structure, one can roughly observe a four-peaked shape whose maxima can be found at about 0.7, 2.8, 7.2 and 11.0 eV. On the contrary, the experimental Al 3s band is comparable intensity at E_F as the Al 3p band and shows a rounded parabolic-like shape towards high binding energies; as mentioned above, this can appear weakly structured owing to a slight oxide contribution in the higher-binding-energy part of the band.

4.2. Conduction-band distributions

In pure Al, an SK LCAO calculation (Papaconstantopoulos 1986) shows that the conduction band states are s–p–d hybridized although principally s–p near E_F; enhancement in p and d partial DOS exists respectively at about 5.5, 7.5 and 8.5 eV from E_F. The Al experimental curve presents three features labelled A, B and C in the same energy ranges; thus, feature A which is intense corresponds to an increase in the p-state distribution whereas features B and C correspond to p–d increases.

The curves presented in figure 2 have been obtained by transmission (curves 1, 3 and 6) or yield (curves 2, 4 and 5) experiments; in the latter case, the oxide contribution to the spectra, if present, is expected to be higher than in the experiments carried out through the samples. Curves 2 and 3 show weakly structured shapes; peak A present at $E_F - 5.5$ eV in pure Al is hardly noticeable, and this indicates changes in the hybridization in the alloys. For i-$Al_{86}Mn_{14}$ and d-$Al_{80}Mn_{20}$ phases, an important broad peak, labelled F, is observed at about $E_F - 9.5$ eV. As mentioned just above, the curve corresponding to d-$Al_{80}Mn_{20}$ might contain an oxide contribution; indeed, a sharp peak is noticed at $E_F - 9$ eV in the Al_2O_3 curve but at $E_F - 10.5$ eV the Al_2O_3 curve displays a clear minimum which is not seen in the curves related to the quasi-crystalline phases. This emphasizes that oxide contamination ought to be faint in both quasi-crystalline samples. Thus, the broad feature F is characteristic of the quasi-crystalline structural state, indicating a reinforcement of the p-state distribution in the $E_F - 9.5$ eV energy range, i.e. a change in hybridization with respect to the related crystalline alloys. This feature seems to be higher in the icosahedral quasi-crystalline phase than in the decagonal phase. In the alloys, at E_F, the behaviour of the empty p DOS is the same as that of the occupied Al 3p and Al 3s DOSs; the intensity decreases when going from crystalline (14 at.% Mn) to icosahedral (14 at.% Mn), decagonal (20 at.% Mn) and amorphous phases (14 at.% Mn) (table 3). This confirms once more the opening of a small gap at E_F with increasing Mn content in the alloys whatever the structural state may be.

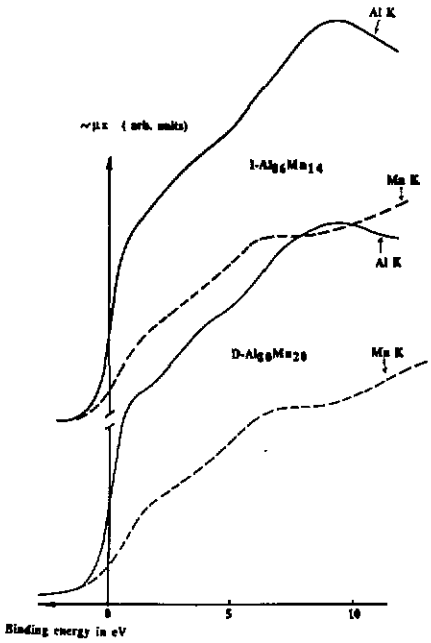

Figure 8. Empty p-state distributions for d-$Al_{80}Mn_{20}$ (lower curves) and for i-$Al_{86}Mn_{14}$ (upper curves). The two sets of curves are arbitrarily shifted along the μx axis.

As calculated by Papaconstantopoulos 1986, the Mn p conduction states show a slight peak at about 0.3 eV from E_F, then a plateau over 1.5 eV and a monotonic increase in intensity followed by an abrupt step at about $E_F - 8.5$ eV. The experimental curve (figure 4) is consistent with this calculation; the peak and the plateau correspond to the flat edge, and the monotonic increase to the flat part of the curve just before a progressive increase in intensity which starts at approximately $E_F - 7.5$ eV.

Fujiwara's (1989, 1990) calculation displays an empty p DOS for the Al–Mn alloys but unfortunately only from E_F to $E_F - 5.2$ eV. Over this energy range, a sharp peak is predicted at 1.2 eV and then the intensity increases continuously. This is also consistent with the shapes of curves 2–7 in figure 4. However, the curves corresponding to i-$Al_{73}Mn_{21}ASi_6$, i-$Al_{86}Mn_{14}$ and d-$Al_{80}Mn_{20}$ alloys clearly exhibit a broad feature F at about $E_F - 6.5$ eV which is absent in the curves related to the crystalline or amorphous phases. As concluded before for the Al p DOS, this feature F appears to be characteristic of the quasi-crystalline state revealing changes in hybridization of the p conduction states with respect to the crystalline and amorphous counterparts.

Finally, in Al–Mn or Al–Mn–Si alloys, the conduction states of Al p and Mn p character are completely mixed over the experimental energy range; at E_F and close to it, Al p states appear to be predominant for all alloys, as shown in figure 8 for two quasi-crystalline phases.

5. Conclusion

In this paper we have reported the analysis, through SXES and SXAS experiments, of valence and conduction band state distributions in a series of quasi-crystalline (icosahedral and decagonal phases) Al–Mn and Al–Mn–Si alloys compared with their crystalline or amorphous counterparts.

Mn d states are found at E_F and close to it interact with Al 3s–3p states. For the lowest Mn concentrations (14–20 at.%), the Al 3s–3p and Mn 3d–4s states of the valence band are totally hybridized near E_F. However, since the partial Al 3s and Al 3p subbands are progressively, and in a different way, repelled from E_F as the Mn concentration is enhanced in the alloy (above 20 at.%), this induces progressively a differentiation of the states and the (Mn d)–(Al s–p) interaction tends to be less achieved. Therefore, whatever may be the Mn concentration and the structural state of the alloys that we have analysed, the Al 3s–3p hybrization is total over the valence band.

As the Fermi level is not located at the maximum of the Mn 3d band, there is no experimental evidence for the existence of a virtual bound state in the quasi-crystalline alloys as was predicted by several workers. The same is true for the crystalline or amorphous counterparts.

At E_F, the empty Al p DOS behave as the occupied Al 3sp. This is experimentally evidenced by the progressive opening of a small gap at E_F as the Mn content is increased in the alloy for a given Mn concentration; the gap is higher in the quasi-crystal phases than in the corresponding crystalline phases. The empty Mn p and Al p distributions overlap; Al p states seem to prevail close to E_F and are of noticeable intensity at $E_F - 9.5$ eV in the quasi-crystalline phases.

References

Belin E and Traverse A 1991 *J. Phys.: Condens. Matter* **3** 2157

Berger C, Gozlan A, Lasjaunias J C, Fourcaudot G and Cyrot-Lackmann F 1991 *Phys. Scr.* **T35** 90

Bruwiller P A, Shen Y, Schnatterly S E and Poon S J 1987 *Phys. Rev.* B **36** 7347

Cyrot-Lackmann F, Mayou D and Nguyen Manh D 1988 *Mater. Sci. Eng.* **99** 245

Dubois J M, Janot Ch and Pannetier J 1986 *Phys. Lett.* **15A** 177

Ederer D L, Schaefer L, Tsang K L, Zhang C H, Calcott T A and Arakawa E T 1988 *Phys. Rev.* B **37** 8594

Fujiwara T 1989 *Phys. Rev.* B **40** 942

—— 1990 *J. Non Cryst. Solids* **117–8** 844

Fujiwara T and Yokokawa T 1991 *Phys. Rev. Lett.* **66** 333

Gozlan A, Berger C, Fourcaudot G, Grieco J C and Cyrot-Lackmann F 1990 *Solid State Commun.* **73** 417

Gozlan A, Berger C, Fourcaudot G, Omari R, Lasjaunias J C and Préjean J J 1991 *Phys. Rev.* B **44** p 575

Harmelin M 1988 *Quasicrystalline Materials (Institut Laue–Langevin–CODEST Workshop)* ed C Janot and J-M Dubois (Singapore: World Scientific) p 19

Macko D, Hudàk O and Hajko V Jr 1989 *Phys. Lett.* **136A** 327

Marcus M A 1986 *Phys. Rev.* B **34** 5981

Matsuda T, Sakabe Y, Ohara I and Mizutami U 1990 *J. Non-Cryst. Solids* **117–8** 804

Mayou D, Maret M and Pasturel A 1988 *Quasicrystalline Materials (Institut Laue–Langevin–CODEST Workshop)* ed C Janot and J M Dubois (Singapore: World Scientific) p 409

Mayou D, Nguyen Manh D, Pasturel A and Cyrot-Lackmann F 1986 *Phys. Rev.* B **33** 3384

Papaconstantopoulos D A 1986 *Handbook of the Band Structure of Elemental Solids* (New York: Plenum) pp 94, 205

Shechtman D, Blech I, Gratias D and Cahn J W 1984 *Phys. Rev. Lett.* **53** 1951

Smith A P and Ashcroft N W 1987 *Phys. Rev. Lett.* **59** 1365

Traverse A, Dumoulin L, Belin E and Sénémaud C 1988 *Quasicrystalline Materials (Institut Laue–Langevin–CODEST Workshop)* ed C Janot and J M Dubois (Singapore: World Scientific) p 399

Wagner J L, Mong K M and Poon S J 1989 *Phys. Rev.* B **39** 8091